

# Tropical Temperature and Precipitation Responses to Large Volcanic Eruptions: Observations and AMIP5 Simulations

A. MEYER, D. FOLINI, U. LOHMANN, AND T. PETER

*ETH Zürich, Zurich, Switzerland*

(Manuscript received 10 January 2015, in final form 10 November 2015)

## ABSTRACT

Tropical land mean surface air temperature and precipitation responses to the eruptions of El Chichón in 1982 and Pinatubo in 1991, as simulated by the atmosphere-only GCMs (AMIP) in phase 5 of the Coupled Model Intercomparison Project (CMIP5), are examined and compared to three observational datasets. The El Niño–Southern Oscillation (ENSO) signal was statistically separated from the volcanic signal in all time series. Focusing on the ENSO signal, it was found that the 17 investigated AMIP models successfully simulate the observed 4-month delay in the temperature responses to the ENSO phase but simulate somewhat too-fast precipitation responses during the El Niño onset stage. The observed correlation between temperature and ENSO phase (correlation coefficient of 0.75) is generally captured well by the models (simulated correlation of 0.71 and ensemble means of 0.61–0.83). For precipitation, mean correlations with the ENSO phase are  $-0.59$  for observations and  $-0.53$  for the models, with individual ensemble members having correlations as low as  $-0.26$ . Observed, ENSO-removed tropical land temperature and precipitation decrease by about  $0.35\text{ K}$  and  $0.25\text{ mm day}^{-1}$  after the Pinatubo eruption, while no significant decrease in either variable was observed after El Chichón. The AMIP models generally capture this behavior despite a tendency to overestimate the precipitation response to El Chichón. Scatter is substantial, both across models and across ensemble members of individual models. Natural variability thus may still play a prominent role despite the strong volcanic forcing.

## 1. Introduction

Explosive volcanic eruptions have major impacts on the climate system, on time scales of a few months to a few years. Upon a strong eruption, sulfur dioxide ( $\text{SO}_2$ ) may reach the lower stratosphere, where it is converted into aqueous sulfuric acid droplets that scatter short-wave and absorb infrared radiation and overall reduce the global mean surface air temperature. The volcanic aerosol may affect the formation of precipitation in several ways. Decreases in surface air temperatures lead to reduced evaporation and decreases in tropospheric column-integrated water vapor (Randel et al. 1996). Since precipitation is directly linked to evaporation, global mean precipitation decreases after a strong volcanic eruption (Robock and Liu 1994). Once the stratospheric volcanic aerosol has been advected or sedimented into the upper troposphere, it may also

influence cloud microphysical processes (Kübbeler et al. 2012; Cirisan et al. 2013) and consequently precipitation. Stratospheric aerosol particles that form after a large volcanic eruption have typical stratospheric residence times on the order of a year. After returning to the troposphere, they may reside there for days up to a few weeks (Thomason and Peter 2006) and during this time alter the lifetime and properties of clouds in the upper and midtroposphere. The response to radiative forcings is physically less constrained for precipitation than for temperature (Allen and Ingram 2002). Accordingly, the signal-to-noise ratio of precipitation responses to volcanic eruptions is thought to be lower than for surface air temperature (Robock and Liu 1994). In addition, a variety of dynamical feedback processes complicate matters further. The volcanic aerosol may induce vertical and horizontal heating gradients. These can affect stratospheric and tropospheric dynamical processes (see, e.g., Graf et al. 1993; Ramachandran et al. 2000; Stenchikov et al. 2002), which may affect the distribution of precipitation.

Observational studies indicate, for example, significant decreases in global and tropical-land-area

---

Corresponding author address: A. Meyer, ETH Zürich, Universitaetsstrasse 16, 8092 Zurich, Switzerland.  
E-mail: angela.meyer@env.ethz.ch

TABLE 1. CMIP5 models evaluated in this study including their resolution (number of degrees in longitude  $n_{lon}$  by number of degrees in latitude  $n_{lat}$ ). CESM1(CAM5), GISS-E2-R (p3), MIROC5, and MRI-CGCM3 calculate gas-to-aerosol conversion and aerosol heating as a function of the simulated atmospheric state variables (“online”).

Model index	Model	$n_{lon} \times n_{lat}$	Ensemble members	Stratospheric aerosol	SSTs and sea ice concentration	Reference
1	BCC_CSM1.1	128° × 64°	3	Ammann et al. (2003)	Taylor et al. (2000)	Wu et al. (2010)
2	CCSM4	288° × 192°	6	Ammann et al. (2003)	Hurrell et al. (2008)	Gent et al. (2011)
3	CESM1(CAM5)	288° × 192°	2	Online	Hurrell et al. (2008)	Neale et al. (2010)
4	GFDL CM3	144° × 90°	5	Stenchikov et al. (1998)	Taylor et al. (2000)	Donner et al. (2011)
5	GISS-E2-R (p1)	144° × 90°	6	Koch et al. (2011)	Rayner et al. (2003)	Shindell et al. (2013)
6	GISS-E2-R (p3)	144° × 90°	6	Online	Rayner et al. (2003)	Shindell et al. (2013, 2006)
7	IPSL-CM5A-MR	144° × 143°	3	Lean (2009)	Taylor et al. (2000)	Dufresne et al. (2013)
8	MIROC5	256° × 128°	2	Online	Taylor et al. (2000)	Watanabe et al. (2010); Takemura et al. (2005)
9	MPI-ESM-LR	192° × 96°	3	Stenchikov et al. (1998)	Taylor et al. (2000)	Stevens et al. (2013)
10	MPI-ESM-MR	192° × 96°	3	Stenchikov et al. (1998)	Taylor et al. (2000)	Stevens et al. (2013)
11	MRI-CGCM3	320° × 160°	3	Online	Taylor et al. (2000)	Yukimoto et al. (2011)
12	NorESM1-M	144° × 96°	3	Ammann et al. (2003)	Hurrell et al. (2008)	Bentsen et al. (2012)
13	IPSL-CM5A-LR	96° × 96°	6	Lean (2009)	Taylor et al. (2000)	Dufresne et al. (2013)
14	FGOALS-s2	128° × 108°	3	Sato et al. (1993)	Taylor et al. (2000)	Bao et al. (2013)
15	BCC_CSM1.1(m)	320° × 160°	3	Ammann et al. (2003)	Taylor et al. (2000)	Wu et al. (2010)
16	CanAM4	128° × 64°	4	Sato et al. (1993)	Hurrell et al. (2008)	von Salzen et al. (2013)
17	GFDL-HIRAM-C180	576° × 360°	3	Stenchikov et al. (1998)	Rayner et al. (2003)	Zhao et al. (2009)

precipitation following the June 1991 eruption of Mount Pinatubo (Trenberth and Dai 2007; Gu and Adler 2011). No significant reduction was observed after the eruption of El Chichón in April 1982, during which an estimated 40% of the amount of SO<sub>2</sub> released during the Pinatubo eruption (18.5 ± 4 Mt) was emitted into the lower stratosphere (Guo et al. 2004; Krueger et al. 2008). Climate simulation studies suggest significant decreases in global and tropical-land-area mean precipitation following the eruptions of Toba about 74 000 years ago (Robock et al. 2009; Timmreck et al. 2012) and of Pinatubo in 1991 (Broccoli et al. 2003), as well as based on composites of several volcanic eruptions (Robock and Liu 1994; Joseph and Zeng 2011; Schneider et al. 2009). Geoengineering has taken an interest in these violent events as observable, potential proxies to estimate the consequences of climate engineering via injection of sulfate into the stratosphere. In this overall context, it is of interest to examine the response of current-generation climate models to the eruptions of Pinatubo and El Chichón.

Iles and Hegerl (2014) studied the responses to volcanic eruptions simulated by atmosphere–ocean coupled climate models in phase 5 of the Coupled Model Intercomparison Project (CMIP5). They found that the models simulate significant global precipitation reductions and that the reductions are largest in the tropics.

The aim of our study is to analyze how well the 17 atmosphere-only models in phase 5 of the Atmospheric Model Intercomparison Project (AMIP5) simulate the observed surface air temperature and precipitation

responses to the eruptions of El Chichón (17°N) in 1982 and Mount Pinatubo (15°N) in 1991. The study is complementary to that of Iles and Hegerl (2014) in two respects: first, in terms of the simulation data examined (AMIP instead of CMIP—i.e., using prescribed, observation-based sea surface temperature data) and second, in that we remove the ENSO signal interfering with the volcano signal (see below) from both observations and model data. Iles and Hegerl (2014) removed it only from the observations and relied on statistical averaging out for the model data.

We focus on the El Chichón and Pinatubo events as they were by far the strongest eruptions after 1979, when satellite-based estimates of precipitation became available for global analysis. We focus on tropical land areas as precipitation reductions after low-latitude volcanic eruptions have been found to affect the tropical regions (20°N–20°S) in particular, which has been related to a weakening or contraction of the Hadley circulation (Robock and Liu 1994; Trenberth and Dai 2007; Schneider et al. 2009).

Identifying potential surface climate effects of volcanic aerosol is complicated by the fact that recent eruptions took place concurrently with warm phases of El Niño–Southern Oscillation (ENSO). During such a warm phase, heat is transported from the ocean to the atmosphere in volcanically quiescent times, so surface air temperatures are enhanced while precipitation over tropical land regions decreases, as precipitation shifts from the land to the ocean (Trenberth et al. 2002). Thus, the influence of ENSO partially masks the effects of the

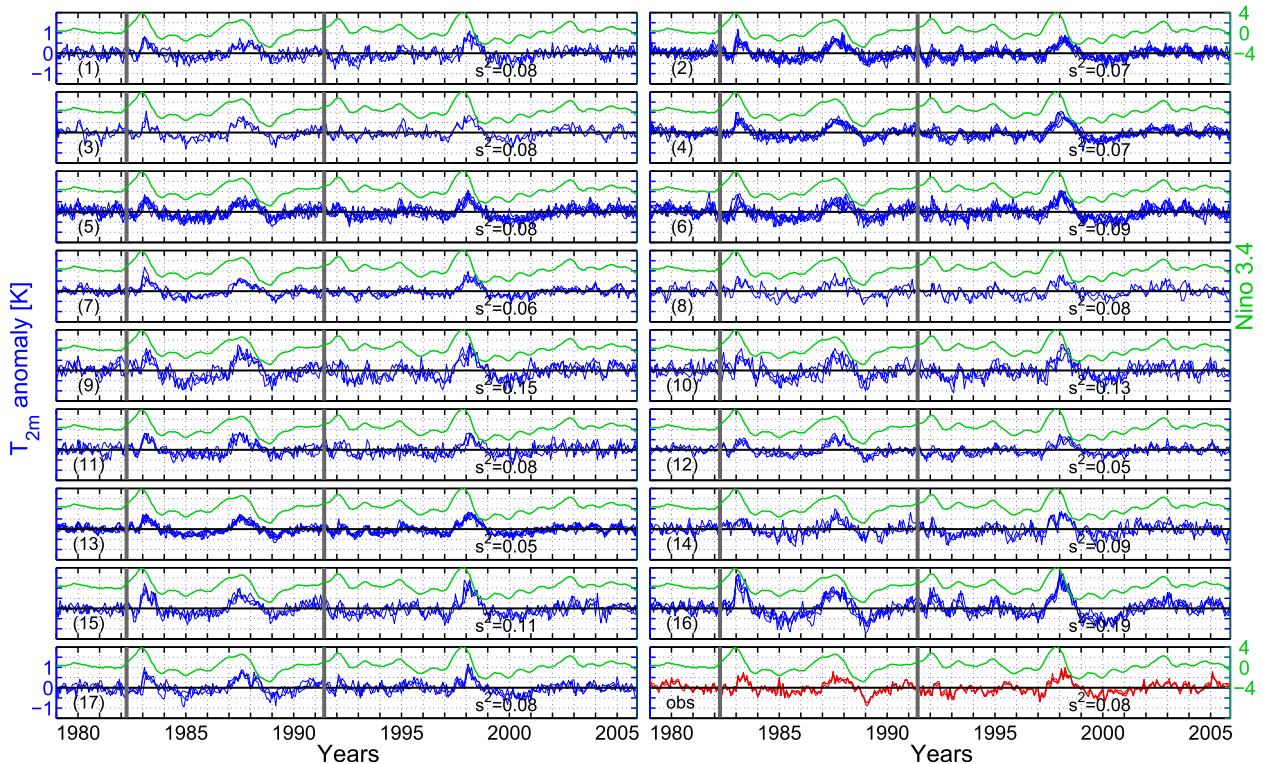


FIG. 1. Filtered  $T_{2m}$  and the Niño-3.4 index. Numbers 1–17 identify the models by the model indices provided in Table 1, and “obs” refers to the three observed filtered  $T_{2m}$  time series. The gray bars indicate the eruptions of El Chichón (April 1982) and Pinatubo (June 1991). The time series variance  $s^2$  ( $K^2$ ) is provided as an ensemble mean for each model and as a mean over the observational datasets.

volcanic aerosol in surface temperature and precipitation time series. Over tropical land regions, for example, an El Niño phase and a strong volcanic eruption will each induce a precipitation reduction while having counteracting effects on surface air temperatures. When studying the surface climate effects of large volcanic eruptions, it is necessary, therefore, to disentangle the volcanic and the ENSO influences.

In our AMIP5 data, we achieve this separation by applying the statistical lag-correlation/regression analysis method presented by Gu and Adler (2011), who investigated volcanic and ENSO signatures in the Global Precipitation Climatology Project (GPCP), version 2.1 (Adler et al. 2003).

The objectives of our study are 1) to determine the time lags of the temperature and precipitation responses to changes in the ENSO phase based on observations and AMIP5 model simulations, 2) to investigate the observed and simulated sensitivity of the surface climate responses to the ENSO phase, and 3) to compare the magnitudes of the observed and the simulated post-eruptive temperature and precipitation anomalies corrected for the ENSO contribution. We go

beyond the work of Gu and Adler (2011) by investigating these questions for AMIP model simulations and for three different observational datasets of surface air temperature and precipitation.

## 2. Data and methods

### a. Temperature observations

Observed 2-m surface air temperatures were obtained from 1) the Global Historical Climatology Network (GHCN) and the Climate Anomaly Monitoring System (CAMS), version 3.01 (Fan and van den Dool 2008); 2) the University of Delaware’s air temperature dataset (UDeI), version 3.01 (Willmott and Matsuura 1995); and 3) the University of East Anglia Climatic Research Unit temperature dataset (CRU TS), version 3.20 (Harris et al. 2014). These datasets contain global monthly station data interpolated to a  $0.5^\circ \times 0.5^\circ$  grid. Because there are no satellite data of precipitation available prior to 1979, this year was chosen as the start year for the present study. We chose 2005 as the last assessed year for reasons explained below.

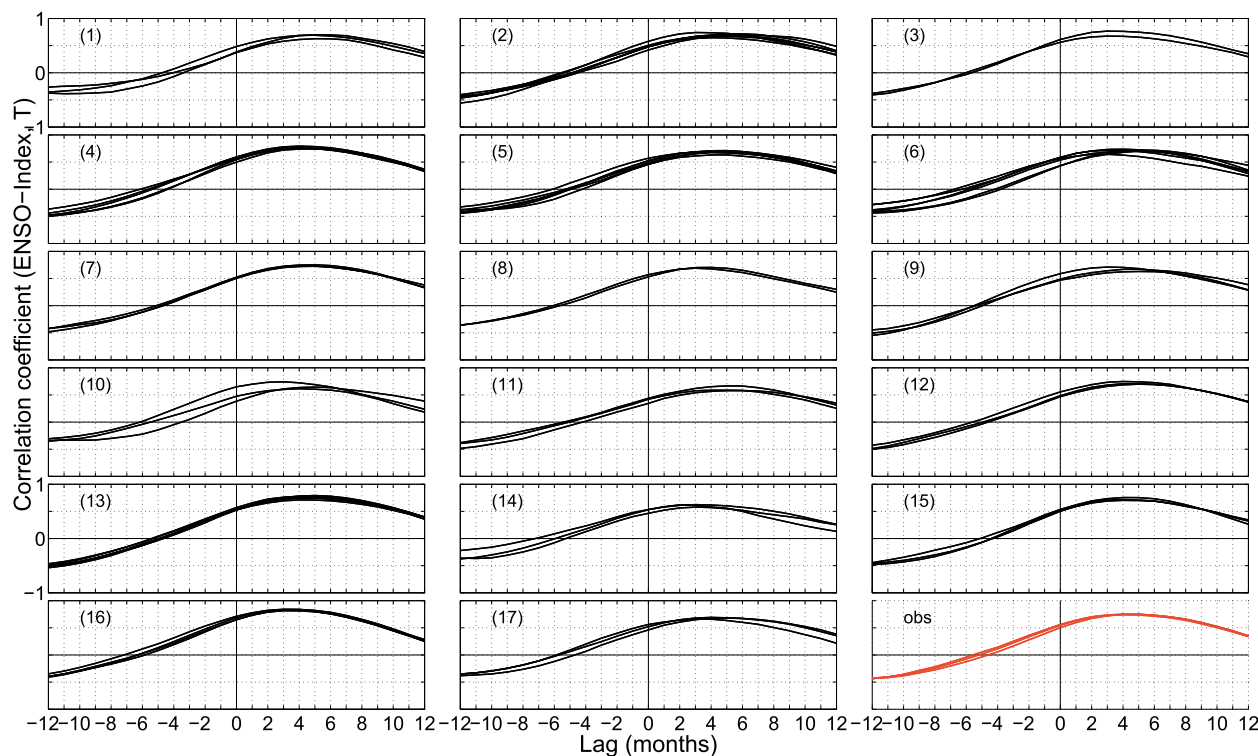


FIG. 2. Shown on the y axis is the Pearson correlation coefficient between filtered  $T_{2m}$  time series over tropical land areas and the Niño-3.4 index for different time lags. The x axis provides the lags (months). Positive lags indicate that the temperature curve reaches its max later than the Niño-3.4 curve. Different curves in each panel indicate the different ensemble members of the corresponding model. Numbers 1–17 identify the models by the model indices provided in Table 1, and “obs” refers to the three observed filtered  $T_{2m}$  time series.

### b. Precipitation observations

Observational data of tropical precipitation over land for years 1979–2005 are taken from three sources: 1) the GPCP, version 2.2 (Adler et al. 2003); 2) the Climate Prediction Center Merged Analysis of Precipitation (CMAP), version 1201 (Xie and Arkin 1997); and 3) the January 2011 version of the Precipitation Reconstruction Over Land dataset (PRECL; Chen et al. 2002). All three datasets provide gridded global monthly mean precipitation at  $2.5^\circ \times 2.5^\circ$  spatial resolution. The GPCP and CMAP datasets are merged satellite and surface rain gauge estimates, while the PRECL is rain gauge based only.

### c. Model data

All simulated data come from the atmosphere-only twentieth-century CMIP5 simulations which have been run with observed sea surface temperatures (SSTs) and sea ice concentrations (CMIP5 experiment 3.3, referred to as AMIP5; Taylor et al. 2012). This ensures that the GCMs are subject to historically correct El Niño/La Niña phases.

Table 1 provides an overview of the 17 models whose simulations we analyzed in this study. We considered

only GCMs for which at least two ensemble members are available and that account for volcanic forcing. Ensemble sizes range from 2 to 6 members, as shown in Table 1. Altogether, we have analyzed 64 ensemble members. For many of the models considered here, the atmosphere-only simulations have been run only for years after 1979 or before 2005. For that reason, our study is based on the years 1979–2005.

Different stratospheric aerosol forcing datasets have been used by the modeling groups, as CMIP5 does not provide emission data for volcanic aerosols. We have compared the three stratospheric aerosol optical depth (AOD) datasets most commonly used in the 17 models. The one by Sato et al. (1993) contains the stratospheric AOD at 550 nm. The Stenchikov et al. (1998) dataset provides stratospheric AOD in the 442–625-nm solar band, while the stratospheric AOD of Ammann et al. (2003) is provided at 500 nm. The Ammann et al. (2003) and Stenchikov et al. (1998) datasets only extend until December 1999. The stratospheric AOD time series of Sato et al. (1993) and Stenchikov et al. (1998) are very similar in the tropical mean, whereas clear differences exist in comparison to Ammann et al. (2003), whose peak tropical mean stratospheric AOD is about 150%

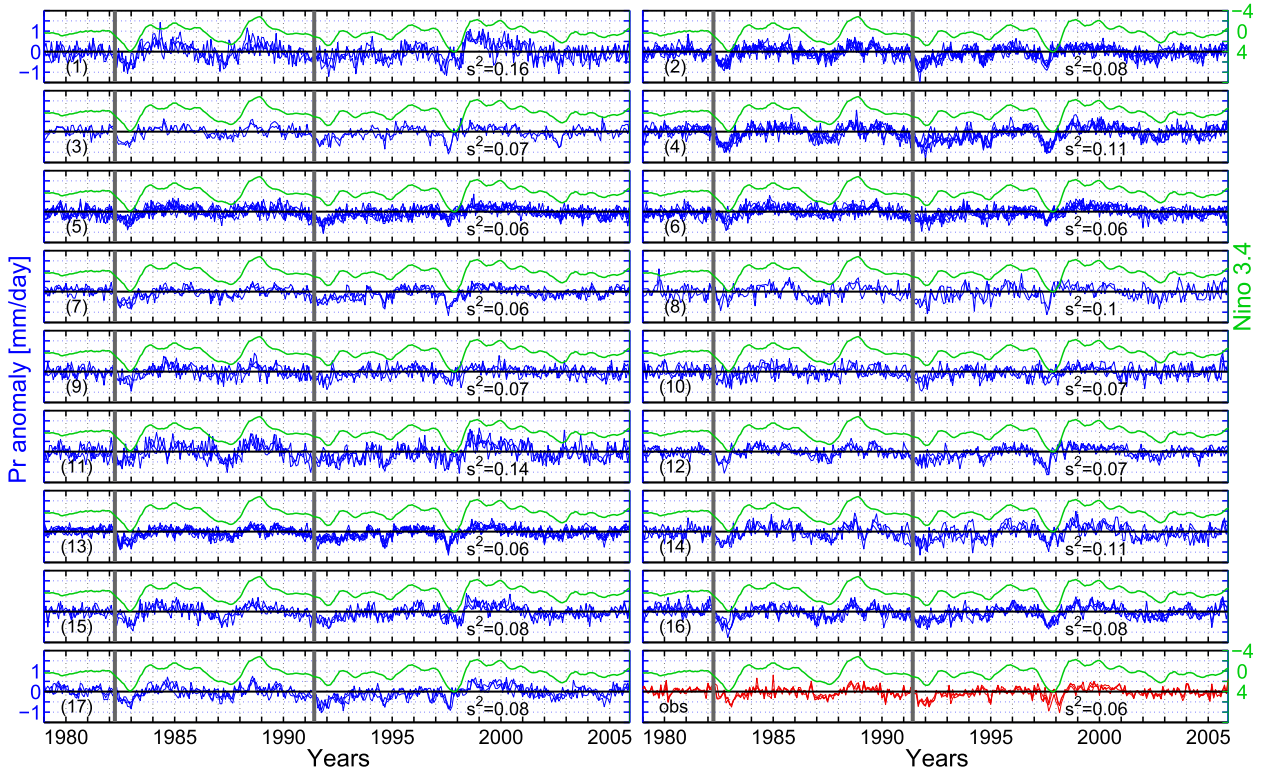


FIG. 3. As in Fig. 1, but for filtered precipitation. The time series variance  $s^2$  [(mm day $^{-1}$ ) $^2$ ] is provided as an ensemble mean for each model and as a mean over the observational datasets.

that of the former two datasets after both eruptions and whose stratospheric AOD decay times exceed those of the other two datasets.

#### d. Choice of post-eruptive periods

We studied 1-yr post-eruptive periods because the volcanic aerosol had a stratospheric residence time on the order of a year in the case of the El Chichón and Pinatubo events. Post-eruptive periods from June 1982 to May 1983 (El Chichón) and from August 1991 to July 1992 (Mt. Pinatubo) were chosen to account for the time needed for the formation of aqueous H<sub>2</sub>SO<sub>4</sub> aerosol droplets from the SO<sub>2</sub> that gathered in the lower stratosphere after the eruptions (Thomason and Peter 2006). We repeated the analysis also for a 2-yr post-eruptive period but obtained largely the same results (not shown in the following).

#### e. ENSO removal

Gu and Adler (2011) suggested that the El Niño/La Niña signal may be removed in the tropics by making use of its strong correlation with tropical land 2-m surface air temperatures  $T_{2m}$  or precipitation. We refer to this procedure as ENSO removal. Our study follows the ENSO removal method outlined by Gu and Adler

(2011). Similar ENSO removal procedures have been applied by Robock and Mao (1995), Trenberth and Dai (2007), Chen et al. (2008), and Joseph and Zeng (2011).

In practical terms, we proceed as follows, for both our three observational and 64 AMIP5 model datasets. The Niño-3.4 index, which is the time series of monthly mean SST anomalies averaged over the tropical Pacific (5°N–5°S, 120°–170°W), was used to represent the ENSO phase. The index was computed from observed SSTs of Taylor et al. (2000). We interpolated all datasets bilinearly to a T63 grid (1.9° × 1.9°) for comparability. Then, at each grid point, we constructed time series of surface air temperature anomalies. We computed the tropical mean as a 20°N–20°S area-weighted average, detrended the time series, and removed the seasonal cycle by subtracting monthly climatologies based on volcanically largely unperturbed times (from April 1979 to March 1982, from April 1985 to March 1991, and from April 1995 to March 2005). We will refer to the detrended and deseasonalized time series as the filtered  $T_{2m}$  time series subsequently. Pearson correlation coefficients  $R$  of each filtered  $T_{2m}$  time series with the Niño-3.4 index were determined. This was done using only the volcanically largely unperturbed time periods as provided above (from April 1979 to March 1982, from

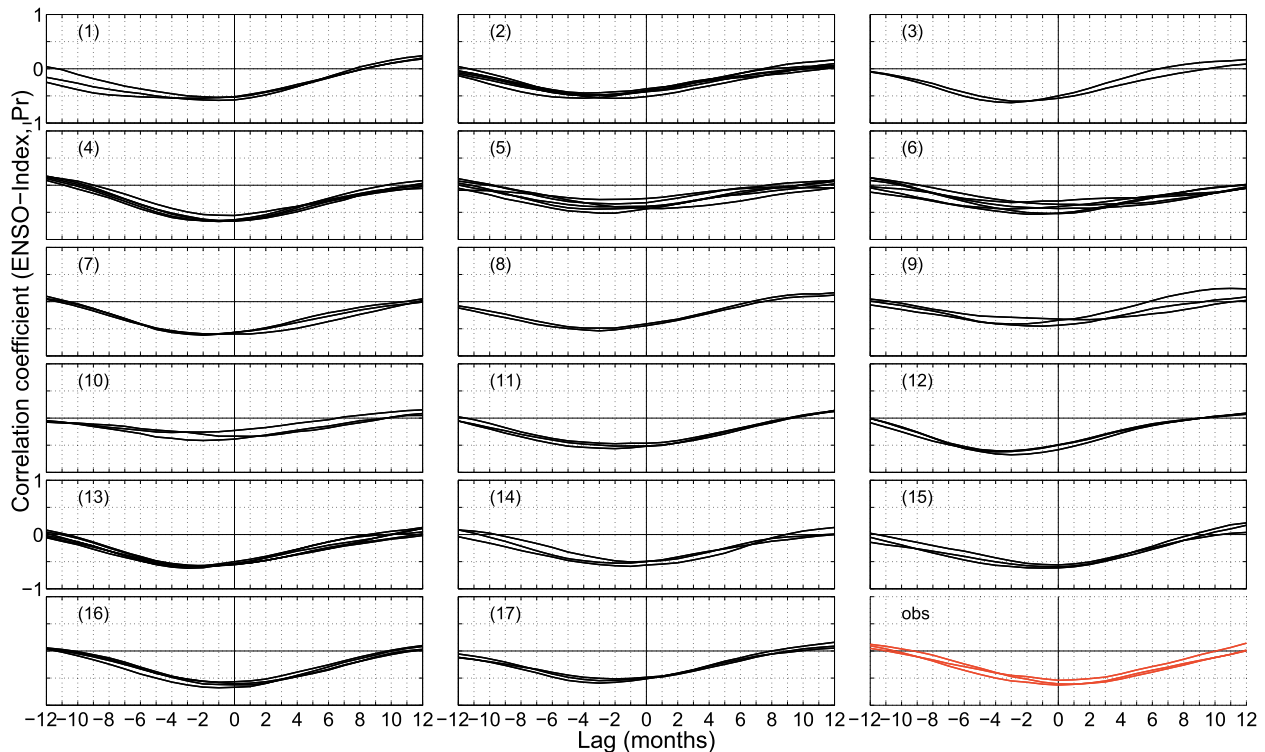


FIG. 4. As in Fig. 2, but for filtered precipitation.

April 1985 to March 1991, and from April 1995 to March 2005). The filtered  $T_{2m}$  time series were shifted with respect to the Niño-3.4 index by time lags of up to 12 months, and a correlation coefficient was computed for each lag. The lag that corresponded to the (in absolute terms) maximal correlation coefficient was taken to be the mean response time of the filtered  $T_{2m}$  time series to the ENSO phase over tropical land areas.

For each filtered  $T_{2m}$  time series, we removed the ENSO signal by first performing a linear regression of the filtered time series shifted by its lag with regard to the Niño-3.4 index. The regression provided an estimated filtered time series:

$$\hat{T}_{2m}(t) = \beta_0 + \beta_1 \text{Niño}3.4(t - \text{lag}).$$

We obtained the ENSO-removed residual temperature by subtracting the estimate from the filtered  $T_{2m}$  time series:

$$T_{2m}^{\text{ENSO removed}}(t) = T_{2m}(t) - \hat{T}_{2m}(t).$$

The regression coefficients were computed based on the volcanically unperturbed periods previously mentioned.

In an analogous manner, the lag-correlation/regression analysis was applied to the three precipitation observation time series and to all of the 64 ensemble members individually.

We note that nonlinear ENSO effects remain poorly understood. By adopting a linear model for the relationship between the ENSO phase and filtered  $T_{2m}$  (or precipitation), we assume that the ENSO phase is not significantly affected by climate responses to volcanic eruptions. As will become clear based on the datasets shown below, linear models appropriately describe the relationship between the Niño-3.4 index and filtered  $T_{2m}$  (or precipitation) for the 1979–2005 time period considered in our study, as they can explain a large fraction of the variance induced in the filtered  $T_{2m}$  and precipitation.

### 3. Results

#### a. Lags and correlations (tropical-land-area mean)

Shown in Fig. 1 are the filtered  $T_{2m}$  for the different observational (red) and simulation (blue) datasets and the Niño-3.4 index. There is some correlation between the filtered  $T_{2m}$  and the ENSO time series if the apparent lag between the two time series is properly taken into account. Comparing both time series in Fig. 1, the temperature response apparently follows the ENSO phase with a time lag of a few months both in the observations and in most ensemble members.

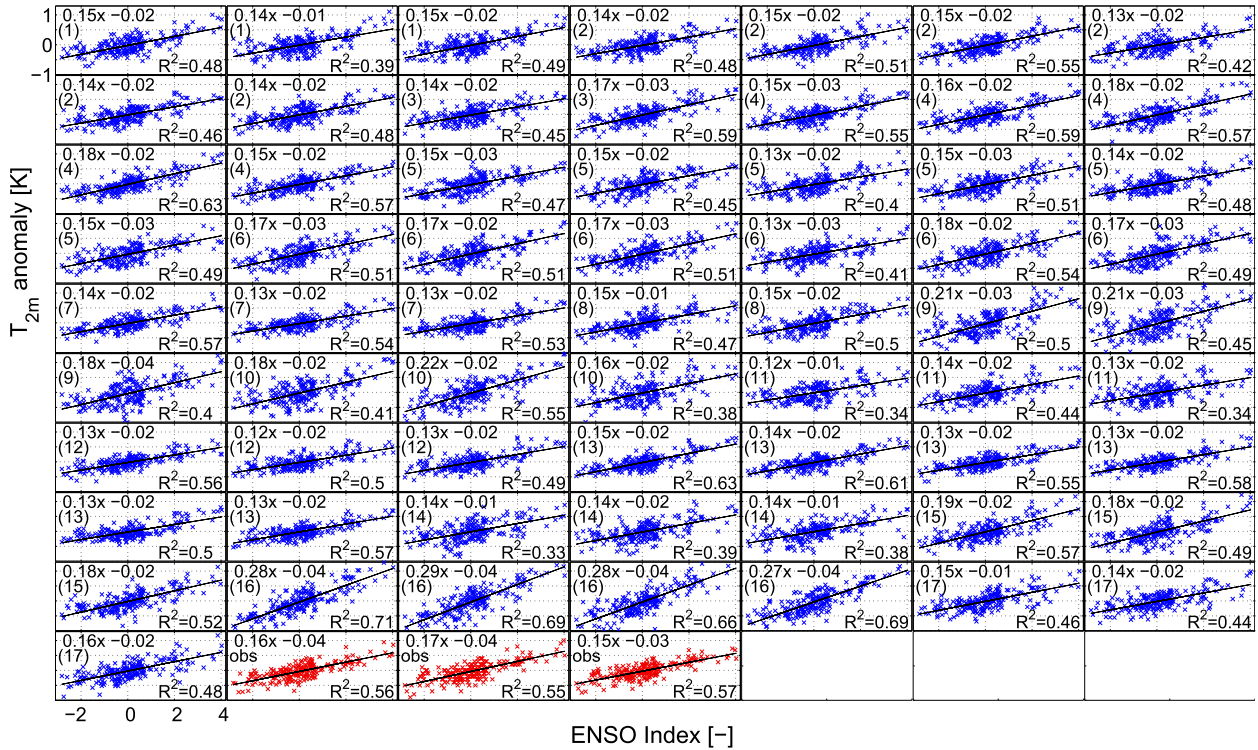


FIG. 5. Regression of lag-shifted filtered  $T_{2m}$  on the Niño-3.4 index. To identify the models, the numbers in parentheses indicate the model indices as provided in Table 1.

Figure 2 quantifies the correlation strength (i.e.,  $R$ ) as a function of the number of months by which the respective temperature time series is shifted relative to the ENSO index. The lags are well defined, as each of the correlation functions is monotonously increasing toward a single maximum.

The lags of the observation-based time series are 4 months (GHCN CAMS and UDel) and 5 months (CRU TS). Those of the model-based time series range from 2 to 7 months with a mean of 4.3 months. Figure 2 also illustrates that for most models the scatter in time lag is small among the ensemble members.

The correlation coefficients between observed lag-shifted filtered temperature and the ENSO index are 0.74 (UDeI) and 0.75 (GHCN CAMS and CRU TS). The simulated correlation coefficients range from 0.58 to 0.84 among the 64 ensemble members with a mean simulated correlation coefficient of 0.71. The strongest temperature–ENSO correlation is simulated by CanAM4 (ensemble mean of 0.83; model index 16), while the weakest correlation is simulated by MRI-CGCM3 and FGOALS (ensemble mean of 0.61 in each model; model indices 11 and 14, respectively).

Figure 3 illustrates the correlation between the Niño-3.4 index and the filtered precipitation. When comparing the onset times of ENSO events, such as the developing

phase of the 1982/83 El Niño event at the beginning of 1982 or the 1997/98 El Niño developing phase at the beginning of 1997, it becomes clear that the observed and the simulated precipitation responses occur with a near-zero time lag. In several models, such as MIROC5 and the IPSL-CM5A-LR (model indices 8 and 13, respectively), the precipitation over tropical land areas seems to respond more sensitively to changes in the ENSO phase than is observed, in particular during El Niño onset phases. These models simulate precipitation minima before the ENSO index reaches its maximum value during the 1991/92 El Niño period. This may imply a too-rapid shift of the simulated convective activity from the tropical land regions toward the ocean.

As shown in Fig. 4, the observed and simulated filtered precipitation time series are significantly negatively correlated with the ENSO phase. Among the 64 ensemble members, the simulated lags range from  $-4$  to  $+2$  months with a mean lag of  $-1.8$  months. The observed precipitation responds to the ENSO phase with a time lag of zero months (GPCP and PRECL) or one month (CMAP). This finding is in agreement with Gu and Adler (2011), who also determined a zero lag using an earlier version of the GPCP dataset. The observed mean precipitation reacts much faster to ENSO phase changes than  $T_{2m}$  over tropical land regions, which

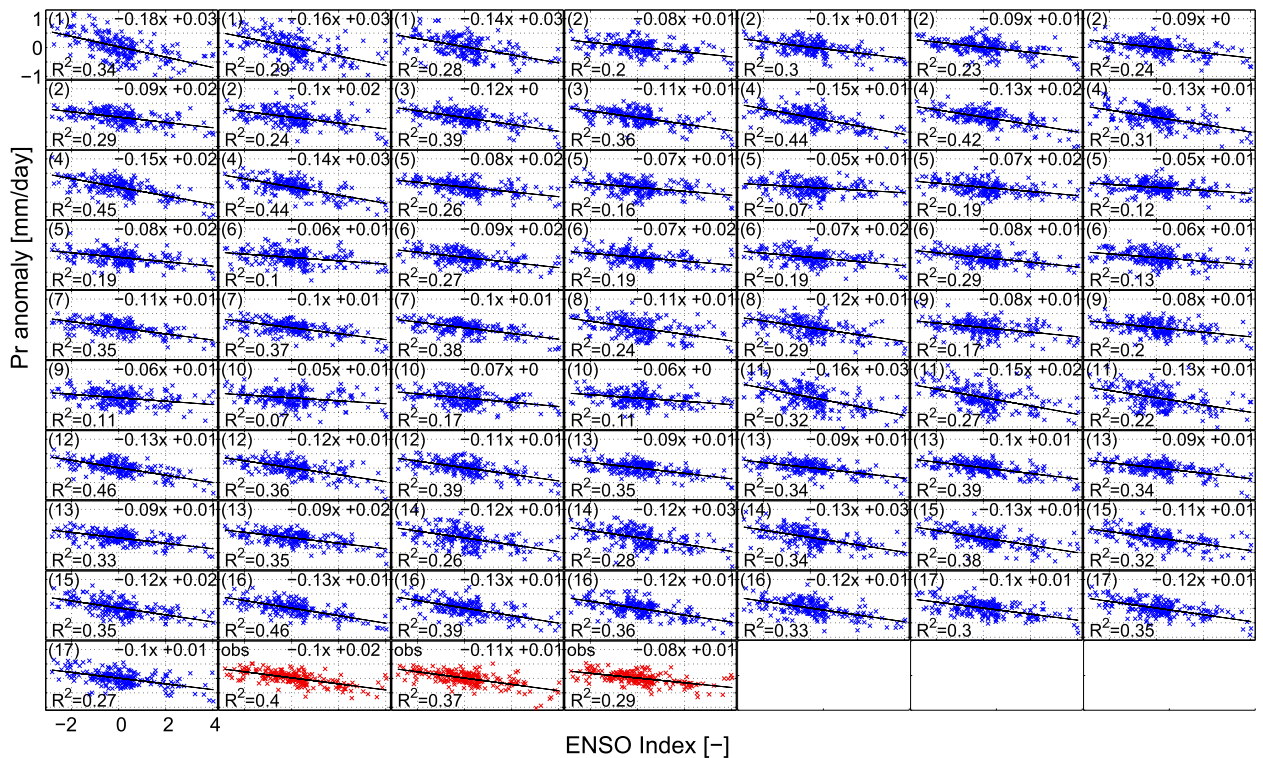


FIG. 6. Regression of lag-shifted filtered tropical mean precipitation over land on the Niño-3.4 index. To identify the models, the numbers in parentheses indicate the model indices as provided in Table 1.

is in agreement with Gu and Adler (2011). The latter study explained this observation by arguing that adjustments of the surface energy budget in response to ENSO phase changes take place more slowly than precipitation responses. The observed behavior (near-instantaneous precipitation response and delayed  $T_{2m}$  response over tropical land regions) is successfully simulated by all 17 evaluated models, even though in most of the models the precipitation over tropical land areas responds too sensitively to a developing El Niño phase.

The correlation of the lag-shifted filtered observed precipitation with the Niño-3.4 index is  $-0.63$ ,  $-0.61$ , and  $-0.54$ , respectively, in the GPCP, CMAP, and PRECL datasets. The mean correlation over the 64 ensemble members is  $-0.53$  (maximum and minimum values of  $-0.68$  and  $-0.26$ ), so AMIP5 tends to underestimate the ENSO–precipitation correlation strength over tropical land regions.

The relationship between lag-shifted filtered  $T_{2m}$  and the ENSO phase can be assumed to be linear to a good approximation, as shown in Fig. 5. The regression lines indicate that the observed  $T_{2m}$  increases by about  $0.16^{\circ}\text{C}$  per unit of Niño-3.4 index. Most of the models simulate temperature responses in agreement with this observed ratio, whereas CanAM4 (model index 16) clearly

overestimates it. About 56% of the variance in the filtered observed  $T_{2m}$  is explained by the linear regression on the Niño-3.4 index, as indicated by the coefficients of determination provided in Fig. 5. Many models simulated ENSO–temperature relationships with values of  $R^2$  somewhat lower than observed, whereas CanAM4 simulates a somewhat too high  $R^2$  because of the strong coupling of its simulated  $T_{2m}$  to the ENSO phase.

The observed negative relationship between precipitation and the ENSO phase can be estimated well by a linear regression line, as shown in Fig. 6. According to the three observational datasets of precipitation, the filtered precipitation is reduced by  $0.1\text{ mm day}^{-1}$  per unit of Niño-3.4 index. The majority of the models successfully simulate a similar ratio. About 35% of the observed variance in filtered precipitation is explained by the regression. The simulated  $R^2$  values range from 7% to 46% among the ensemble members.

#### b. ENSO-removed temperature and precipitation (tropical-land-area mean)

Figure 7 provides the  $T_{2m}^{\text{ENSO removed}}$  time series (i.e., filtered  $T_{2m}$  after the ENSO signal removal by lag correlation/regression as explained above). The time series are 12 months shorter at both ends as compared to

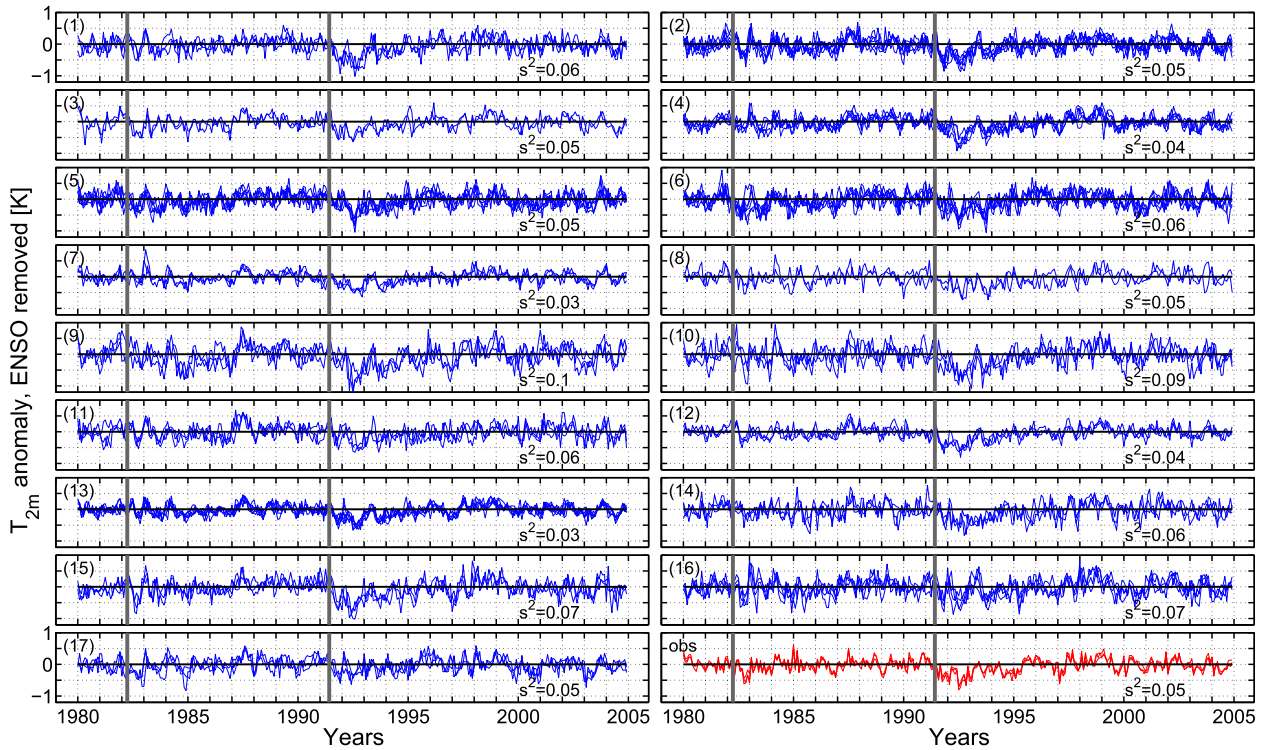


FIG. 7. Residual ENSO-removed  $T_{2m}$  (i.e.,  $T_{2m}^{\text{ENSO removed}}$ ). Model indices, volcanic eruption times, and time series variances are indicated as in Fig. 1.

before the ENSO removal (Fig. 1) because our approach for determining the time lags allows for shifting by up to  $\pm 12$  months.

As can be seen, removing the ENSO contributions significantly reduced the variance of the filtered  $T_{2m}$  time series for all models and in all observational datasets, as expected. The mean variance of the three  $T_{2m}^{\text{ENSO removed}}$  observational datasets was reduced from 0.08 to 0.05  $\text{K}^2$ , for example.

Focusing now on our original goal, the impact of the El Chichón and Pinatubo eruptions as seen in appropriately treated time series, mean temperature reductions of about 0.4 and 0.6 K are observed over tropical land areas after the El Chichón and Pinatubo eruptions in late 1982 and the second half of 1992, respectively, in agreement with Gu and Adler (2011, their Figs. 3b and 8b).

The variances in the filtered precipitation time series were likewise significantly reduced by the ENSO removal for all models and the observational datasets, as shown in Fig. 8. The mean precipitation observed over tropical land areas is clearly reduced by up to  $0.3 \text{ mm day}^{-1}$  following the Pinatubo eruption, whereas the observed precipitation response to the eruption of El Chichón is more ambiguous, in agreement with Gu and Adler (2011, their Figs. 2b and 7b).

Figure 9 shows the ranges of  $T_{2m}^{\text{ENSO removed}}$  and precipitation anomalies after ENSO removal for each ensemble member. The whiskers indicate the maximum and minimum anomalies.

Before determining the significance of the observed and simulated post-eruptive  $T_{2m}^{\text{ENSO removed}}$  and precipitation reductions, we found that  $T_{2m}^{\text{ENSO removed}}$  and the residual precipitation time series are significantly auto-correlated at a lag of one month. To remove the auto-correlation, we prewhitened the time series by transforming them according to  $y'_t = (y_t - r_1 y_{t-1}) / (1 - r_1)$  (von Storch and Navarra 1993; Wang and Swail 2001), where  $r_1$  is the lag-1 autocorrelation coefficient. A two-sided Mann-Whitney test was performed on the prewhitened time series of ensemble-mean  $T_{2m}^{\text{ENSO removed}}$  and residual ensemble-mean precipitation anomalies to test the null hypothesis that the mean of the post-eruptive monthly anomalies is not significantly different from the mean of the control period at the 95% level.

The anomalies shown in Fig. 9 are means over the above 12-month post-eruptive periods. As shown in Fig. 9, the observed  $T_{2m}^{\text{ENSO removed}}$  and ENSO-removed precipitation dropped significantly by about 0.35 K and  $0.25 \text{ mm day}^{-1}$  after the Pinatubo eruption. This is in good agreement with the Niño-3.4-removed filtered surface air temperature and precipitation responses

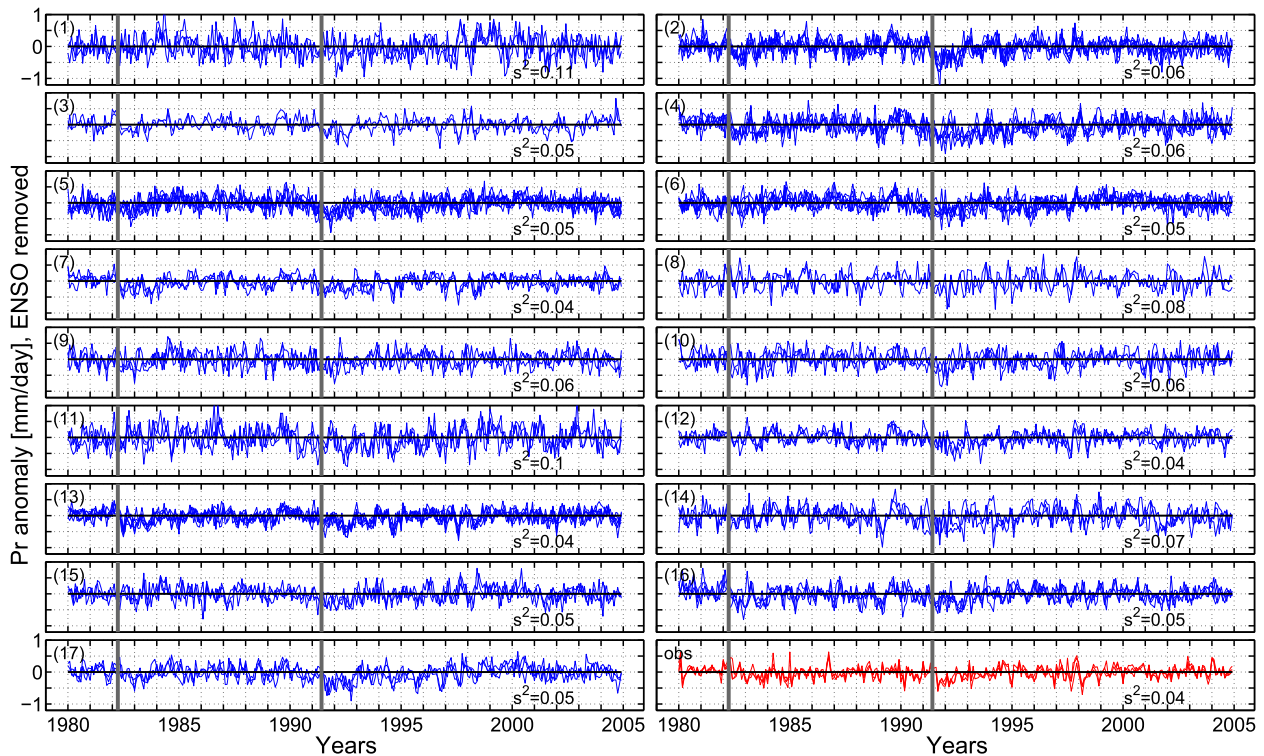


FIG. 8. Residual ENSO-removed precipitation. Model indices, volcanic eruption times, and time series variances are indicated as in Fig. 1.

obtained by Gu and Adler (2011, their Figs. 7b and 8b) based on an earlier version of the GPCP dataset. The observed  $T_{2m}^{\text{ENSO removed}}$  and precipitation reductions of about 0.17 K and  $0.05 \text{ mm day}^{-1}$  in the year after the El Chichón eruption are not statistically significant.

The AMIP5 models generally simulate  $T_{2m}^{\text{ENSO removed}}$  and ENSO-removed precipitation responses in agreement with the magnitude of the observed responses. There is, however, a tendency for overestimating the observed (nonsignificant) precipitation response to the El Chichón eruption over tropical land areas. Also, there is large scatter in the simulated anomalies, both across models and across ensemble members within a single model. The latter is interesting as it may point to a still significant role of natural variability even in the presence of strong volcanic forcing. Of course, other interpretations are possible as well, from model deficiencies to insufficient quality of the ENSO removal.

Figure 10 shows the simulated and observed anomalies of all ensemble members. The mean and standard deviation of the simulated surface temperature and precipitation anomalies, taken over all ensemble members of all 17 models, are  $-0.08 \pm 0.11 \text{ K}$  and  $-0.12 \pm 0.09 \text{ mm day}^{-1}$  for the El Chichón eruption

and  $-0.29 \pm 0.11 \text{ K}$  and  $-0.26 \pm 0.10 \text{ mm day}^{-1}$  for Pinatubo. This corresponds to signal-to-noise ratios of 0.7 and 1.3 for the anomalies in  $T_{2m}^{\text{ENSO removed}}$  and precipitation in the case of El Chichón eruption and of 2.6 for both the  $T_{2m}^{\text{ENSO removed}}$  and the precipitation anomalies for Pinatubo.

The ranges (maximum–minimum) of the simulated  $T_{2m}^{\text{ENSO removed}}$  and precipitation anomalies over all ensemble members and models are 0.52 K and  $0.40 \text{ mm day}^{-1}$  (El Chichón) and 0.49 K and  $0.51 \text{ mm day}^{-1}$  (Pinatubo). The large scatter in the simulated temperature and precipitation anomalies among the 64 ensemble members illustrates the small ratio of volcanic signal to model internal variability (and to model-to-model variability) in the AMIP5 simulations.

It is interesting to note that there is no apparent relation between the strength of the  $T_{2m}^{\text{ENSO removed}}$  response and that of the ENSO-removed precipitation response.

The Pinatubo eruption was 2–3 times larger than the eruption of El Chichón in terms of the stratospheric  $\text{SO}_2$  input (Thomason and Peter 2006). Figure 10 suggests that the stratospheric AOD increase and the reduction in evaporation following the El Chichón eruption were not large enough to cause a response in  $T_{2m}^{\text{ENSO removed}}$  and

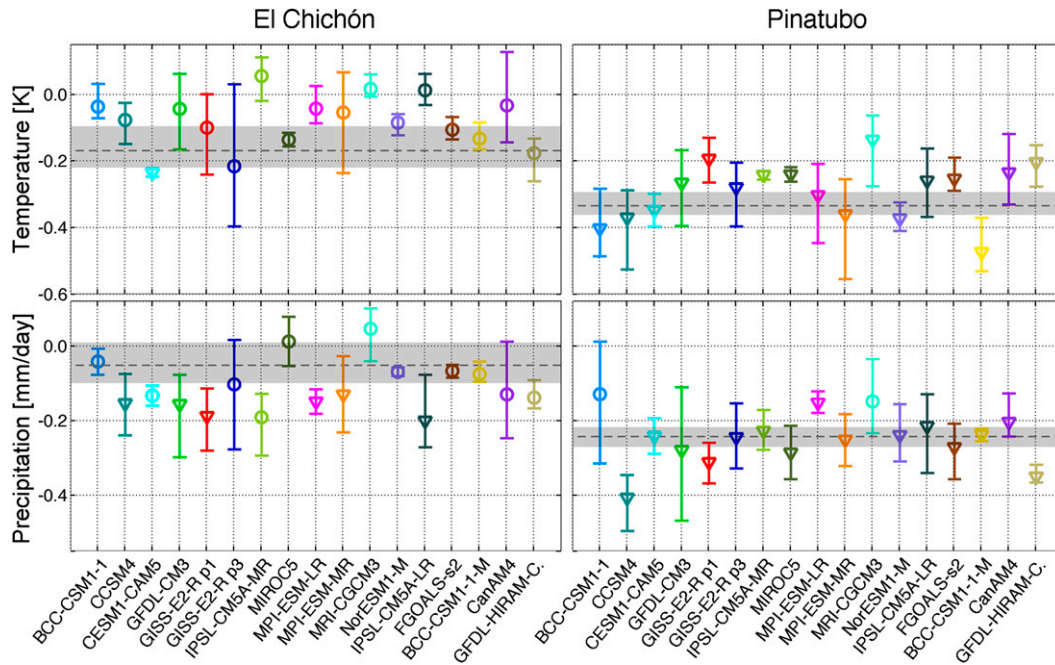


FIG. 9. Simulated anomalies in  $T_{2m}^{ENSO\ removed}$  and ENSO-removed precipitation after the El Chichón and Pinatubo eruptions, averaged from June 1982 to May 1983 and from August 1991 to July 1992, respectively. Ensemble-mean anomalies are marked by a triangle when significantly (at the 95% level) below the model’s control-period mean or by a circle otherwise. Ensemble min and max anomalies are marked by the upper and lower whisker edges. Gray shadings denote the ranges of observed post-eruptive anomalies.

ENSO-removed precipitation beyond the level of natural variability.

**4. Conclusions**

We have investigated surface air temperature and precipitation responses to the eruptions of El Chichón in April 1982 and Mount Pinatubo in June 1991 over tropical land areas, as simulated by 17 atmosphere-only GCMs in phase 5 of the Coupled Model Intercomparison Project (CMIP5).

The objectives of our study were to validate the time lags and coupling strengths of the simulated surface climate responses to changes in the ENSO phase and to validate the observed and the simulated post-eruptive temperature and precipitation anomalies over tropical land areas by comparison to observed temperature and precipitation.

Focusing on the responses over tropical land regions, we found the following:

- All models successfully simulate surface air temperature responses delayed by a few months relative to the ENSO phase (on average 4.3 months), which agrees well with the observed 4–5-month delay.
- The strong positive correlation observed between mean temperatures and the ENSO phase (correlation

coefficient of 0.75) is generally captured well by the models (simulated correlation of 0.71). There is, however, considerable scatter in the simulated correlation strength across models (ensemble means of 0.61–0.83).

- The observed precipitation response lags the ENSO phase by 0–1 months. Most of the models appear to simulate a somewhat too-fast precipitation response during the El Niño onset (mean simulated lag of –1.8 months). This may be related to a too-rapid shift of simulated convective activity toward the ocean.
- The models tend to underestimate the observed correlation strength between precipitation and ENSO phase (mean correlation of –0.59). The mean simulated correlation coefficient is –0.53. Simulated correlations of ensemble members range as low as –0.26.
- The observed relationship between ENSO phase, as measured by the Niño-3.4 index, and temperature (or precipitation) can be considered linear to a reasonably good approximation for 1979–2005. The models successfully capture this linearity, though in the case of temperature typically at lower values of  $R^2$ .
- The observed mean temperature and precipitation increase by  $0.16^{\circ}\text{C}$  and  $0.1\text{ mm day}^{-1}$  per unit of Niño-3.4 index. Many but not all models simulate

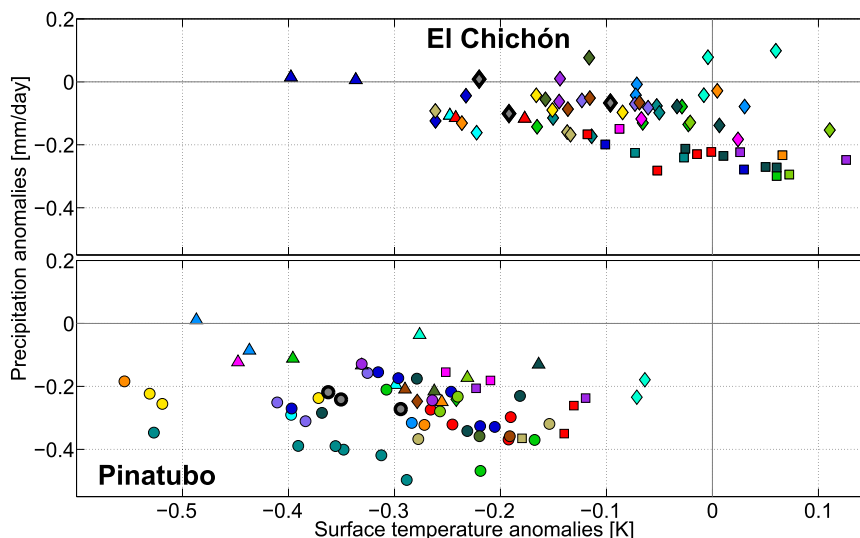


FIG. 10. Simulated anomalies in  $T_{2m}^{\text{ENSO removed}}$  and ENSO-removed precipitation anomalies of the 64 ensemble members, averaged from June 1982 to May 1983 (El Chichón) and from August 1991 to July 1992 (Pinatubo). Observational values are marked by boldface edges. Circles indicate a significant reduction in  $T_{2m}^{\text{ENSO removed}}$  and ENSO-removed precipitation; triangles (squares) mark significant decreases in  $T_{2m}^{\text{ENSO removed}}$  (ENSO-removed precipitation) only. Diamond symbols were chosen when there was no significant post-eruptive decrease in any of the two variables. Significance was tested at the 95% level in all cases. The marker colors indicate the associated model in accordance with the color coding used in Fig. 9.

temperature and precipitation sensitivities in agreement with this finding.

- Observed ENSO-removed temperature and precipitation decreased by about 0.35 K and 0.25 mm day<sup>-1</sup> after the Pinatubo eruption, whereas no significant decrease in either variable was observed after El Chichón. The models generally capture this behavior, though with large scatter. They appear to somewhat overestimate the precipitation response to El Chichón.
- The stratospheric AOD increase and associated reduction in evaporation after the El Chichón eruption seem to not have been large enough to result in temperature or precipitation responses beyond the level of natural variability.

Obviously, the present study is only a first step. An area we did not touch upon is the model physics behind the good or bad agreement between observations and one particular model—or, similarly, the reason for the considerable spread across ensemble members for at least some models. Another question concerns the quality of the ENSO removal. One possible way forward here could be a dedicated modeling study: perform two sets of atmosphere-only model simulations that differ only in the presence or absence of Pinatubo-like eruptions and check

whether the ENSO removal procedure applied here can indeed retrieve the difference signal of the two sets of simulations.

*Acknowledgments.* We thank Christoph Frei for helpful discussions and are grateful to Urs Beyerle for downloading and archiving the CMIP5 datasets. We also thank three anonymous reviewers for their constructive comments on our manuscript. The CMAP, PRECL, and GPCP precipitation data as well as the GHCN and UDel surface air temperature data were provided by NOAA/OAR/ESRL PSD, Boulder, Colorado (<http://www.esrl.noaa.gov/psd/data/gridded/>). The CRU TS air temperature data were provided by the NCAS British Atmospheric Data Centre ([http://browse.ceda.ac.uk/browse/badc/cru/data/cru\\_ts/cru\\_ts\\_3.20/data/](http://browse.ceda.ac.uk/browse/badc/cru/data/cru_ts/cru_ts_3.20/data/)). The dataset of Sato et al. (1993) is available online (<http://data.giss.nasa.gov/modelforce/strataer/>). The Stenchikov et al. (1998) dataset is contained in the ECHAM6 archive. The dataset of Ammann et al. (2003) is provided online (<http://www.ncdc.noaa.gov/paleo/pubs/ammann2003/ammann2003.html>). All of the aforementioned datasets are available for free download. This work was supported by ETH Research Grant CH2-01 11-1 and the Center for Climate Systems Modeling (C2SM).

## REFERENCES

- Adler, R. F., and Coauthors, 2003: The Version-2 Global Precipitation Climatology Project (GPCP) monthly precipitation analysis (1979–present). *J. Hydrometeor.*, **4**, 1147–1167, doi:10.1175/1525-7541(2003)004<1147:TVGPCP>2.0.CO;2.
- Allen, M. R., and W. J. Ingram, 2002: Constraints on future changes in climate and the hydrologic cycle. *Nature*, **419**, 224–232, doi:10.1038/nature01092.
- Ammann, C. M., G. A. Meehl, W. M. Washington, and C. S. Zender, 2003: A monthly and latitudinally varying volcanic forcing dataset in simulations of 20th century climate. *Geophys. Res. Lett.*, **30**, 1657, doi:10.1029/2003GL016875.
- Bao, Q., and Coauthors, 2013: The Flexible Global Ocean–Atmosphere–Land System Model, spectral version 2: FGOALS-s2. *Adv. Atmos. Sci.*, **30**, 561–576, doi:10.1007/s00376-012-2113-9.
- Bentsen, M., and Coauthors, 2012: The Norwegian Earth System Model, NorESM1-M—Part 1: Description and basic evaluation. *Geosci. Model Dev.*, **6**, 687–720, doi:10.5194/gmd-6-687-2013.
- Broccoli, A. J., K. W. Dixon, T. L. Delworth, T. R. Knutson, R. J. Stouffer, and F. Zeng, 2003: Twentieth-century temperature and precipitation trends in ensemble climate simulations including natural and anthropogenic forcing. *J. Geophys. Res.*, **108**, 4798, doi:10.1029/2003JD003812.
- Chen, J., A. D. Del Genio, B. E. Carlson, and M. G. Bosilovich, 2008: The spatiotemporal structure of twentieth-century climate variations in observations and reanalyses. Part I: Long-term trend. *J. Climate*, **21**, 2611–2633, doi:10.1175/2007JCLI2011.1.
- Chen, M., P. Xie, J. E. Janowiak, and P. A. Arkin, 2002: Global land precipitation: A 50-yr monthly analysis based on gauge observations. *J. Hydrometeor.*, **3**, 249–266, doi:10.1175/1525-7541(2002)003<0249:GLPAYM>2.0.CO;2.
- Cirisan, A., P. Spichtinger, B. P. Luo, D. K. Weisenstein, H. Wernli, U. Lohmann, and T. Peter, 2013: Microphysical and radiative changes in cirrus clouds by geoengineering the stratosphere. *J. Geophys. Res.*, **118**, 4533–4548, doi:10.1002/jgrd.50388.
- Donner, L. J., and Coauthors, 2011: The dynamical core, physical parameterizations, and basic simulation characteristics of the atmospheric component AM3 of the GFDL global coupled model CM3. *J. Climate*, **24**, 3484–3519, doi:10.1175/2011JCLI3955.1.
- Dufresne, J.-L., and Coauthors, 2013: Climate change projections using the IPSL-CM5 Earth System Model: From CMIP3 to CMIP5. *Climate Dyn.*, **40**, 2123–2165, doi:10.1007/s00382-012-1636-1.
- Fan, Y., and H. van den Dool, 2008: A global monthly land surface air temperature analysis for 1948–present. *J. Geophys. Res.*, **113**, D01103, doi:10.1029/2007JD008470.
- Gent, P. R., and Coauthors, 2011: The Community Climate System Model version 4. *J. Climate*, **24**, 4973–4991, doi:10.1175/2011JCLI4083.1.
- Graf, H.-F., I. Kirchner, A. Robock, and I. Schult, 1993: Pinatubo eruption winter climate effects: Model versus observations. *Climate Dyn.*, **9**, 81–93, doi:10.1007/BF00210011.
- Gu, G., and R. F. Adler, 2011: Precipitation and temperature variations on the interannual time scale: Assessing the impact of ENSO and volcanic eruptions. *J. Climate*, **24**, 2258–2270, doi:10.1175/2010JCLI3727.1.
- Guo, S., G. J. S. Bluth, W. I. Rose, I. M. Watson, and A. J. Prata, 2004: Re-evaluation of SO<sub>2</sub> release of the 15 June 1991 Pinatubo eruption using ultraviolet and infrared satellite sensors. *Geochem. Geophys. Geosyst.*, **5**, Q04001, doi:10.1029/2003GC000654.
- Harris, I., P. D. Jones, T. J. Osborn, and D. H. Lister, 2014: Updated high-resolution grids of monthly climatic observations—the CRU TS3.10 dataset. *Int. J. Climatol.*, **34**, 623–642, doi:10.1002/joc.3711.
- Hurrell, J. W., J. J. Hack, D. Shea, J. M. Caron, and J. Rosinski, 2008: A new sea surface temperature and sea ice boundary dataset for the Community Atmosphere Model. *J. Climate*, **21**, 5145–5153, doi:10.1175/2008JCLI2292.1.
- Iles, C. E., and G. C. Hegerl, 2014: The global precipitation response to volcanic eruptions in the CMIP5 models. *Environ. Res. Lett.*, **9**, 104012, doi:10.1088/1748-9326/9/10/104012.
- Joseph, R., and N. Zeng, 2011: Seasonally modulated tropical drought induced by volcanic aerosol. *J. Climate*, **24**, 2045–2060, doi:10.1175/2009JCLI3170.1.
- Koch, D., and Coauthors, 2011: Coupled aerosol-chemistry-climate twentieth-century transient model investigation: Trends in short-lived species and climate responses. *J. Climate*, **24**, 2693–2714, doi:10.1175/2011JCLI3582.1.
- Krueger, A., N. Krotkov, and S. Carn, 2008: El Chichon: The genesis of volcanic sulfur dioxide monitoring from space. *J. Volcanol. Geotherm. Res.*, **175**, 408–414, doi:10.1016/j.jvolgeores.2008.02.026.
- Kübbeler, M., U. Lohmann, and J. Feichter, 2012: Effects of stratospheric sulfate aerosol geo-engineering on cirrus clouds. *Geophys. Res. Lett.*, **39**, L23803, doi:10.1029/2012GL053797.
- Lean, J., 2009: Calculations of solar irradiance: monthly means from 1882 to 2008, annual means from 1610 to 2008. Accessed 21 August 2014. [Available online at [http://www.geo.fu-berlin.de/en/met/ag/strat/forschung/SOLARIS/Input\\_data/Calculations\\_of\\_Solar\\_Irradiance.pdf](http://www.geo.fu-berlin.de/en/met/ag/strat/forschung/SOLARIS/Input_data/Calculations_of_Solar_Irradiance.pdf).]
- Neale, R. B., and Coauthors, 2010: Description of the NCAR Community Atmosphere Model (CAM 5.0). NCAR Tech. Note NCAR/TN-486+STR, 274 pp. [Available online at [http://www.cesm.ucar.edu/models/cesm1.0/cam/docs/description/cam5\\_desc.pdf](http://www.cesm.ucar.edu/models/cesm1.0/cam/docs/description/cam5_desc.pdf).]
- Ramachandran, S., V. Ramaswamy, G. L. Stenchikov, and A. Robock, 2000: Radiative impact of the Mount Pinatubo volcanic eruption: Lower stratospheric response. *J. Geophys. Res.*, **105**, 24 409–24 429, doi:10.1029/2000JD900355.
- Randel, D. L., T. J. Greenwald, T. H. Vonder Haar, G. L. Stephens, M. A. Ringerud, and C. L. Combs, 1996: A new global water vapor dataset. *Bull. Amer. Meteor. Soc.*, **77**, 1233–1246, doi:10.1175/1520-0477(1996)077<1233:ANGWVD>2.0.CO;2.
- Rayner, N. A., D. E. Parker, E. B. Horton, C. K. Folland, L. V. Alexander, D. P. Rowell, E. C. Kent, and A. Kaplan, 2003: Global analyses of sea surface temperature, sea ice, and night marine air temperature since the late nineteenth century. *J. Geophys. Res.*, **108**, 4407, doi:10.1029/2002JD002670.
- Robock, A., and Y. Liu, 1994: The volcanic signal in Goddard Institute for Space Studies three-dimensional model simulations. *J. Climate*, **7**, 44–55, doi:10.1175/1520-0442(1994)007<0044:TVSIGI>2.0.CO;2.
- , and J. Mao, 1995: The volcanic signal in surface temperature observations. *J. Climate*, **8**, 1086–1103, doi:10.1175/1520-0442(1995)008<1086:TVSIST>2.0.CO;2.
- , C. M. Ammann, L. Oman, D. Shindell, S. Levis, and G. Stenchikov, 2009: Did the Toba volcanic eruption of ~74 ka B.P. produce widespread glaciation? *J. Geophys. Res.*, **114**, D10107, doi:10.1029/2008JD011652.

- Sato, M., J. E. Hansen, M. P. McCormick, and J. B. Pollack, 1993: Stratospheric aerosol optical depths, 1850–1990. *J. Geophys. Res.*, **98**, 22 987–22 994, doi:10.1029/93JD02553.
- Schneider, D. P., C. M. Ammann, B. L. Otto-Bliesner, and D. S. Kaufman, 2009: Climate response to large, high-latitude and low-latitude volcanic eruptions in the Community Climate System Model. *J. Geophys. Res.*, **114**, D15101, doi:10.1029/2008JD011222.
- Shindell, D., and Coauthors, 2013: Interactive ozone and methane chemistry in GISS-E2 historical and future climate simulations. *Atmos. Chem. Phys.*, **13**, 2653–2689, doi:10.5194/acp-13-2653-2013.
- , G. Faluvegi, N. Unger, E. Aguilar, G. A. Schmidt, D. M. Koch, S. E. Bauer, and J. R. Miller, 2006: Simulations of preindustrial, present-day, and 2100 conditions in the NASA GISS composition and climate model G-PUCCINI. *Atmos. Chem. Phys.*, **6**, 4427–4459, doi:10.5194/acp-6-4427-2006.
- Stenchikov, G. L., I. Kirchner, A. Robock, H.-F. Graf, J. C. Antua, R. G. Grainger, A. Lambert, and L. Thomason, 1998: Radiative forcing from the 1991 Mount Pinatubo volcanic eruption. *J. Geophys. Res.*, **103**, 13 837–13 857, doi:10.1029/98JD00693.
- , A. Robock, V. Ramaswamy, M. D. Schwarzkopf, K. Hamilton, and S. Ramachandran, 2002: Arctic Oscillation response to the 1991 Mount Pinatubo eruption: Effects of volcanic aerosols and ozone depletion. *J. Geophys. Res.*, **107**, 4803, doi:10.1029/2002JD002090.
- Stevens, B., and Coauthors, 2013: Atmospheric component of the MPI-M Earth System Model: ECHAM6. *J. Adv. Model. Earth Syst.*, **5**, 146–172, doi:10.1002/jame.20015.
- Takemura, T., T. Nozawa, S. Emori, T. Y. Nakajima, and T. Nakajima, 2005: Simulation of climate response to aerosol direct and indirect effects with aerosol transport–radiation model. *J. Geophys. Res.*, **110**, D02202, doi:10.1029/2004JD005029.
- Taylor, K. E., D. Williamson, and F. Zwiers, 2000: The sea surface temperature and sea-ice concentration boundary conditions for AMIP II simulations. PCMDI Tech. Rep. 60, 25 pp.
- , R. J. Stouffer, and G. A. Meehl, 2012: An overview of CMIP5 and the experiment design. *Bull. Amer. Meteor. Soc.*, **93**, 485–498, doi:10.1175/BAMS-D-11-00094.1.
- Thomason, L. W., and T. Peter, Eds., 2006: Assessment of stratospheric aerosol properties (ASAP). SPARC Rep. 4, WMO/TD Rep. 1295, 322 pp. [Available online at <http://www.sparc-climate.org/publications/sparc-reports/sparc-report-no4/>.]
- Timmreck, C., H. Graf, D. Zanchettin, S. Hagemann, T. Kleinen, and K. Krüger, 2012: Climate response to the Toba super-eruption: Regional changes. *Quat. Int.*, **258**, 30–44, doi:10.1016/j.quaint.2011.10.008.
- Trenberth, K. E., and A. Dai, 2007: Effects of Mount Pinatubo volcanic eruption on the hydrological cycle as an analog of geoengineering. *Geophys. Res. Lett.*, **34**, L15702, doi:10.1029/2007GL030524.
- , J. M. Caron, D. P. Stepaniak, and S. Worley, 2002: Evolution of El Niño–Southern Oscillation and global atmospheric surface temperatures. *J. Geophys. Res.*, **107**, 4065, doi:10.1029/2000JD000298.
- von Salzen, K., and Coauthors, 2013: The Canadian Fourth Generation Atmospheric Global Climate Model (CanAM4). Part I: Representation of physical processes. *Atmos.–Ocean*, **51**, 104–125, doi:10.1080/07055900.2012.755610.
- von Storch, H., and A. Navarra, Eds., 1993: *Analysis of Climate Variability*, 342 pp.
- Wang, X. L., and V. R. Swail, 2001: Changes of extreme wave heights in Northern Hemisphere oceans and related atmospheric circulation regimes. *J. Climate*, **14**, 2204–2221, doi:10.1175/1520-0442(2001)014<2204:COEWHI>2.0.CO;2.
- Watanabe, M., and Coauthors, 2010: Improved climate simulation by MIROC5: Mean states, variability, and climate sensitivity. *J. Climate*, **23**, 6312–6335, doi:10.1175/2010JCLI3679.1.
- Willmott, C. J., and K. Matsuura, 1995: Smart interpolation of annually averaged air temperature in the United States. *J. Appl. Meteor.*, **34**, 2577–2586, doi:10.1175/1520-0450(1995)034<2577:SIOAAA>2.0.CO;2.
- Wu, T., and Coauthors, 2010: The Beijing Climate Center atmospheric general circulation model: Description and its performance for the present-day climate. *Climate Dyn.*, **34**, 123–147, doi:10.1007/s00382-008-0487-2.
- Xie, P., and P. A. Arkin, 1997: Global precipitation: A 17-year monthly analysis based on gauge observations, satellite estimates, and numerical model outputs. *Bull. Amer. Meteor. Soc.*, **78**, 2539–2558, doi:10.1175/1520-0477(1997)078<2539:GPAYMA>2.0.CO;2.
- Yukimoto, S., and Coauthors, 2011: Meteorological Research Institute Earth System Model version 1 (MRI-ESM1): Model description. Meteorological Research Institute Tech. Rep. 64, 83 pp. [Available online at [http://www.mri-jma.go.jp/Publish/Technical/DATA/VOL\\_64/tec\\_rep\\_mri\\_64.pdf](http://www.mri-jma.go.jp/Publish/Technical/DATA/VOL_64/tec_rep_mri_64.pdf).]
- Zhao, M., I. Held, S.-J. Lin, and G. A. Vecchi, 2009: Simulations of global hurricane climatology, interannual variability, and response to global warming using a 50-km resolution GCM. *J. Climate*, **22**, 6653–6678, doi:10.1175/2009JCLI3049.1.